Uncovering the Local Structure of Amorphous Topological Insulator Bi_2Se_3 with X-ray Scattering

Mitchell Hilbig

A senior thesis submitted to the faculty of
Brigham Young University
in partial fulfillment of the requirements for the degree of

Bachelor of Science

Benjamin Frandsen, Advisor

Department of Physics and Astronomy

Brigham Young University

ABSTRACT

Uncovering the Local Structure
of Amorphous Topological Insulator
Bi_2Se_3 with X-ray Scattering

Mitchell Hilbig
Department of Physics and Astronomy, BYU
Bachelor of Science

Topological insulators are a much-studied class of materials known to exhibit electrical insulation within the bulk and robust conduction on the surface. Normally crystalline in structure, recent proof of amorphous topological insulators exhibiting the same properties as their crystalline counterparts has been identified, challenging prevailing notions about the structural requirements for topological insulators. To gain a deeper understanding of amorphous bismuth selenide (Bi_2Se_3) as the first known amorphous topological insulator, we performed x-ray diffraction experiments on thin films of this material. Using a variety of modeling methods, including reverse Monte Carlo (RMC) simulations, we gained a detailed understanding of the short-range order that remains extant in amorphous Bi_2Se_3 and compared this to its crystalline counterpart. The results provide insight into how the structure of amorphous topological insulators influences the topological state.

Keywords: [Topology, Topological Insulator, Topological Insulators, Amorphous, Amorphous Topological Insulator, Amorphous Topological Insulators, Hall, Spin, Spin Momentum, Spin-Momentum, Spin-Momentum Locking]

ACKNOWLEDGMENTS

We extend our heartfelt thanks to Sinéad M. Griffin, Frances Hellman, Paul Corbae, Manel Molina-Ruiz, Milinda Abeykoon, and Yuanpeng Zhang for their valuable support and collaboration throughout this project.

Contents

Chapter 1

Introduction

1.1 Topological Insulators

Topology is a branch of mathematics concerned with the properties of geometric objects that are preserved under continuous deformation (i.e. bending, twisting, stretching, etc.) [1, 2]. For this research, topology in reference to a physical state describes the preservation of the state despite subjection to physical deformation or the introduction of chemical impurity. Of particular interest in this regard are topological insulators (TIs), a unique class of materials that exhibit electrical insulation in the bulk of the material, and conduction at the surface. Since these materials maintain these properties even when physically deformed or after incurring chemical impurity, they are classified as topologically insulating.

More precisely, this description as topologically insulating refers to the preservation of the set of all allowed energy eigenstates for a given value of electron momentum. This set in momentum space cannot be adiabatically transformed to a topologically trivial trivial set, that of an ordinary insulator, without crossing a set which produces a conducting state at the surface—this state remaining

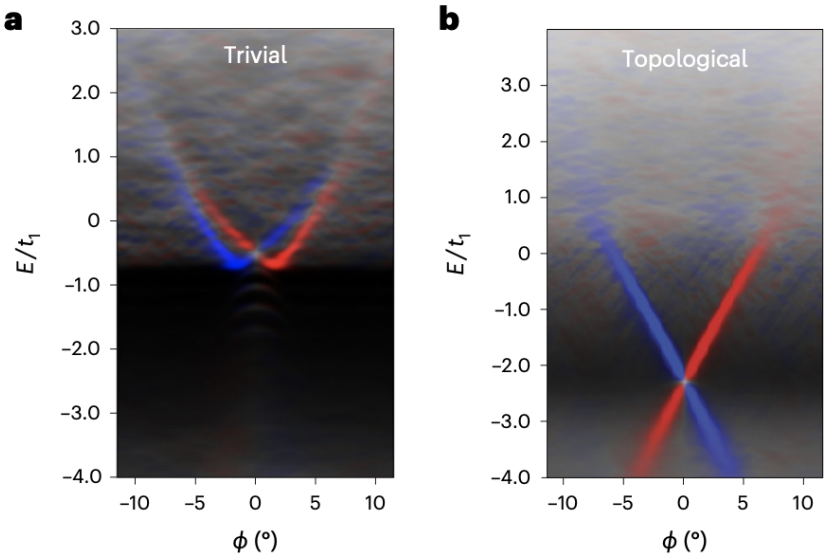

Figure 1.1 Spin-resolved surface spectral function as a function of ϕ for the trivial **(a)** and topological **(b)** phases. The energy is normalized by the hopping amplitude t_1.

intact even despite physical deformation or the introduction of chemical impurity, a combination distinguishing TIs from ordinary insulators and conductors. [3]

Corbae et al. exhibit the distinction between trivial and topological phases in their 2023 work "Observation of spin-momentum locked surface states in amorphous Bi_2Se_3" [4], a figure from which is copied here as Fig. 1.1. In the topological phase, the Dirac point is low in binding energies and the production of a conducting state arises near the Fermi level. No such state is produced in the trivial phase, or in other words, in an ordinary insulator.

1.2 Amorphous Topological Insulators

Theoretical predictions which laid the groundwork for topological insulators date back to 1985, when Volkov and Pankratov described the possibility of such a quantum state [5]. The first physical realization of the topologically insulating state was produced in 2007 by Molenkamp et al with two

dimensional HgTe quantum wells positioned between CdTe layers [6] [7]. Results published in 2008 marked the unveiling of three dimensional topological insulators with Bi_xSb_{1-x} [8], followed by Bi_2Se_3 and Bi_2Te_3 in 2009, demonstrating robust topological insulating properties at higher temperature and in the simplest surface state possible [9] [10].

From the publication of these studies until recently, the vast majority of the theoretical and experimental work revolving around TIs has begun from the starting assumption of a well-ordered crystalline structure. While many studies detail the survival of topological insulation in materials subject to disorder (i.e. materials without perfect crystalline structure in localized sections) [11] [12], the periodic structure of the global material has been assumed as the prerequisite for stabilizing topological insulating states. However, in 2023, Corbae et. al observed instances of spin-momentum locking, a hallmark trait of TIs, within a fully amorphous sample of Bi_2Se_3 for the first time. [4]

Angle-resolved photoemission spectroscopy (ARPES) showed a two-dimensional conducting surface state with strong spin-momentum locking, where spin polarization varied with ARPES detection angle, directly proportional to the plane-wave momentum k. Taking this spin-momentum locking as evidence for a genuine topological surface state in amorphous Bi_2Se_3, this result expands the scope of topological insulators beyond crystalline materials, an advancement that will shape future research in TIs. The discovery of spin-momentum locking within amorphous Bi_2Se_3 challenges conventional understanding of TIs, where previously surface states were assumed to be dependent on crystalline structure.

This discovery came with a paradigm shift in our understanding of topological insulators that required a closer look at the configuration of atoms that make up the amorphous Bi_2Se_3. Although the work by Corbae et al. clearly demonstrates spin-momentum locking and proves the amorphous nature of the Bi_2Se_3 samples they investigated, very little detail about the local arrangement of atoms in amorphous Bi2Se3 could be gleaned from their experimental techniques. Additional studies using specialized techniques designed to probe short-range atomic correlations are needed to

gain a deeper understanding of the structure of amorphous Bi2Se3 and how it can support electronic topological properties.

1.3 Overview

To address this need, we performed x-ray scattering experiments on amorphous films of Bi_2Se_3 at Brookhaven National Laboratory's National Synchrotron Light Source II (NSLSII) in Brookhaven, New York. Comparing this experimentally gathered data to small-box models of crystalline Bi_2Se_3, we have demonstrated that the local arrangement of atoms in amorphous films retains many features of bulk Bi_2Se_3. Specifically, short range order is preserved in the transition from purely crystalline to amorphous Bi_2Se_3. Further, utilizing the reverse Monte-Carlo (RMC) method through Oak Ridge National Laboratory's rmcprofile software, we have simulated large-box models of amorphous Bi_2Se_3, whose structures yields quantitatively similar pair distribution functions (PDF) that the x-ray diffraction data of physical Bi_2Se_3 produced. The detailed information provided by RMC fits confirms the similarities between the local structure of amorphous films and bulk Bi_2Se_3 while also highlighting some important differences between it and the crystalline structure. This could serve as a starting point in producing theoretical frameworks that encompass this broader class of TI. The distribution of specific atom pair distances, as well as bond angles, for the species that make up the material are among the important quantities obtained from this method, producing a clear picture of local structure, and serving as a strong foundation for more sophisticated theoretical works.

Chapter 2

Methods

2.1 Sample Synthesis

Thin films of amorphous Bi_2Se_3 with a thickness of 250 nm were grown and characterized following the procedure in the 2023 Corbae et. al publication [4], through thermal evaporation in a vacuum chamber at $10^{-}9$ torr. Synthesis ocurred at room temperature, using singles sources of elemental Bi and Se. The amorphous structure of the samples was confirmed using high-resolution transmission electron microscopy (TEM), x-ray diffraction, and Raman scattering. TEM verified the absence of crystalline order in amorphous Bi_2Se_3 thin films, by producing diffuse rings in its diffraction patterns, as opposed to sharp Bragg peaks, which would signal the presence of long-range crystalline order. X-ray diffraction patterns and Raman spectroscopy corroborate the TEM result, confirming the disordered structure of the films. The energy dispersive x-ray spectroscopy maps point to uniform distribution of Bi and Se without clustering. Raman scattering induced by a 488 nm laser generated broadened peaks as compared to the crystalline system. Further, speckled results from scanning nanodiffraction indicate lack of crystalline periodicity, while the uniformity of speckles across beam spots imply short range order.

2.2 X-ray Diffraction

X-ray diffraction is the technique we utilized to further extract detailed information about the atomic structure of amorphous Bi_2Se_3. X-ray bombarded samples scatter radiation according to Bragg's law, which dictates that constructive interference between two rays occurs only when the difference between interfering x-ray path-lengths is an integer number of wavelengths. Namely,

$$n\,\lambda = 2\,d\sin\theta \tag{2.1}$$

where n is an integer, λ is x-ray wavelength, d is the distance between atomic planes, and θ is the glancing angle. Fig. 2.1 depicts this relationship for planes composed of sheets of atoms—a good model for simple crystalline structure. Bragg's relationship holds for more complex materials as well, including amorphous Bi_2Se_3, the material of interest for our study. In practice, intensity peaks of constructive interference are received a by detector as shown in Fig. 2.2. The data gathered from this detection are a function of momentum, and are subset of what is called "momentum space" or "reciprocal space." Fourier transformation converts this reciprocal space data into real space data—in other words, the data used in PDFs as described in Section 1.3—and details the probability that an atom will be found a given distance away from any other atom with high precision. This data is far more intuitive to work with, and provides an excellent description of short-range atomic order within a sample. We use PDF data to draw conclusions about amorphous Bi_2Se_3's distinctions and similarities to crystalline Bi_2Se_3.

To obtain the highest quality x-ray diffraction data, we utilized Brookhaven National Laboratory's NSLS II. Fig. 2.2 shows the beamline and detector used to gather data. We compared the information retrieved from NSLS II 5vwith simulations that further elucidate how amorphous matter with strong spin–orbit coupling can sustain spin-momentum locked surface states.

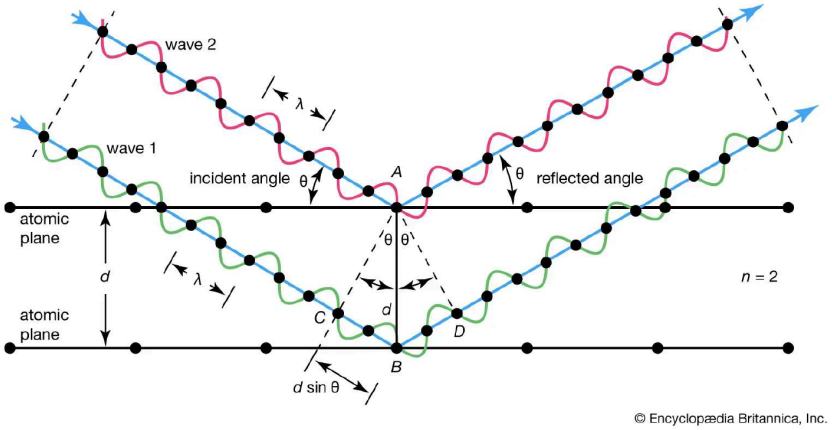

Figure 2.1 Bragg diffraction. *Image: Encyclopædia Britannica, Inc.*

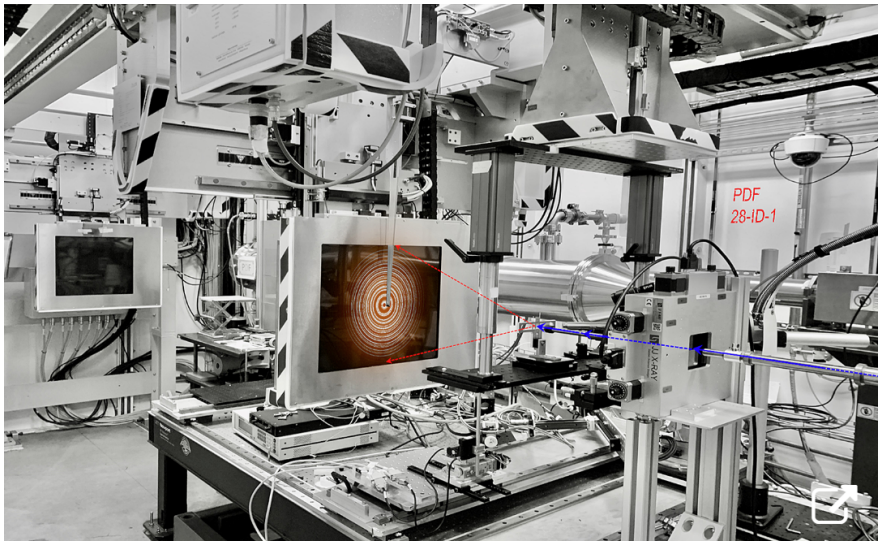

Figure 2.2 Brookhaven National Laboratory's National Synchrotron Light Source II. *Image: Brookhaven National Laboratory*

2.3 Data Analysis

Numerical simulations allow us to further interpret x-ray scattering data. Taking two approaches described as "small-box modeling" and "large box modeling," we expanded our understanding of the short-range correlations within amorphous Bi_2Se_3 by comparing these models to experimentally gathered PDF data gleaned from x-ray diffraction

The small-box approach models crystalline Bi_2Se_3 as small set of atoms, typically under 1000, and assumes a repeating unit cell described by a CIF file—a standardized file format that specifies the exact position of all atoms in a simulated structure. These small-box models offered a valuable approach to compare short range order between expected interatomic correlations that characterize crystalline Bi_2Se_3, and those that characterize its amorphous variant. By deriving PDFs from simulated Bi_2Se_3 crystals, and comparing them to experimentally gathered PDFs for amorphous Bi_2Se_3 slabs, we gained insights into the local atomic arrangements of amorphous Bi_2Se_3.

Comparison involved achieving the best fit between simulated and experimental PDFs by building small-box models containing a variable number of Bi_2Se_3 layers unit cells, both in-plane and out-of-plane, thereby concluding to what extent short-range crystalline order remains extant in an amorphous configuration of Bi_2Se_3. To find the greatest possible fit given the parameters, we aimed to minimize the R_w (weighted residual) value for the fit, given by:

$$\sqrt{\frac{\sum (y_{calc} - y_{obs})^2}{\sum (y_{calc})^2}} \tag{2.2}$$

Through systematic adjustments and comparisons, we identified the structural arrangements from crystalline Bi_2Se_3 that contribute most to the observed PDF patterns in amorphous Bi_2Se_3, evident in correlated peaks and their relative amplitudes. This iterative process enabled us to gain insights into the local atomic arrangements and bonding configurations within the disordered structure, shedding light on the nature of short-range order in this system.

A more detailed approach was then requisite to properly evaluate the discrepancies in the PDF results between the simulated and experimental data. RMC simulations proved to be an effective tool for creating simulated Bi_2Se_3 that produced a PDF with nearly perfect fit to our experimental PDF for amorphous Bi_2Se_3. The RMC method as applied to atomic simulations and PDF fits, is an algorithm that chooses a simulated atom at random, and moves it from its current position to one nearby. A PDF is then calculated for this new configuration, and if the fit improves between the newly calculated PDF for simulated Bi_2Se_3 and the experimentally gathered PDF for amorphous Bi_2Se_3, the move is kept. This process repeats until the simulated PDF reaches the best possible fit to the experimental PDF. The algorithm also incorporates a chance that an unfavorable move is kept, such that the fit does not get stuck in some local minimum that may not truly be best.

By starting with a CIF file describing a large simulated sample of crystalline Bi_2Se_3, and implementing the RMC method through Oak Ridge National Laboratory's rmcprofile program, we arrived at a simulated arrangement of amorphous Bi_2Se_3 that allowed us finer insight into the properties of physical Bi_2Se_3, due to its strong fit with the experimental PDF. From this model, we calculated both the coordination number across 50 Å and the bond angle distributions from zero to 180 degrees, each of which offer a more detailed picture of what atomic correlations exist in amorphous Bi_2Se_3. This information is necessary to lay the groundwork for theoretical descriptions of topological insulators that do not depend on translational symmetry, and will help us to understand why topologically insulating states remain present in amorphous Bi_2Se_3.

Chapter 3

Results

3.1 Model Independent Analysis

Initial inspection of the PDF data gathered for amorphous Bi_2Se_3 revealed short range correlations as expected. Atomic correlations below 30 Å are visible as clear peaks in the PDF data. The gradual suppression of the PDF height with increasing distance indicates a loss of well defined atomic order. Fig. 3.1 shows the order present in the short range, and the loss of order as distance lengthens.

The short range distances between crystalline Bi_2Se_3 atom-pairs are depicted in Fig. 3.2. Near neighbor distances between bismuth-bismuth pairs, bismuth-selenium pairs, and selenium-selenium pairs all contribute radial distribution functions which are summed to obtain the total PDF given in Fig. 3.1. Radial distribution functions are similar to PDFs, but are confined to specific atom pairs. The most relevant near neighbor distances for this study are under 10 Å and account for the largest peaks depicted in Fig. 3.1. Amorphous Bi_2Se_3 shows similar near neighbor correlations. Peaks visible in the inset of Fig. 3.1 are centered closely to the distances expected for crystalline Bi_2Se_3.

The robustness to physical disorder characteristic of crystalline Bi_2Se_3's topological state, even exaggerated to the point of amorphization, speaks to the fact that the topological state is not as

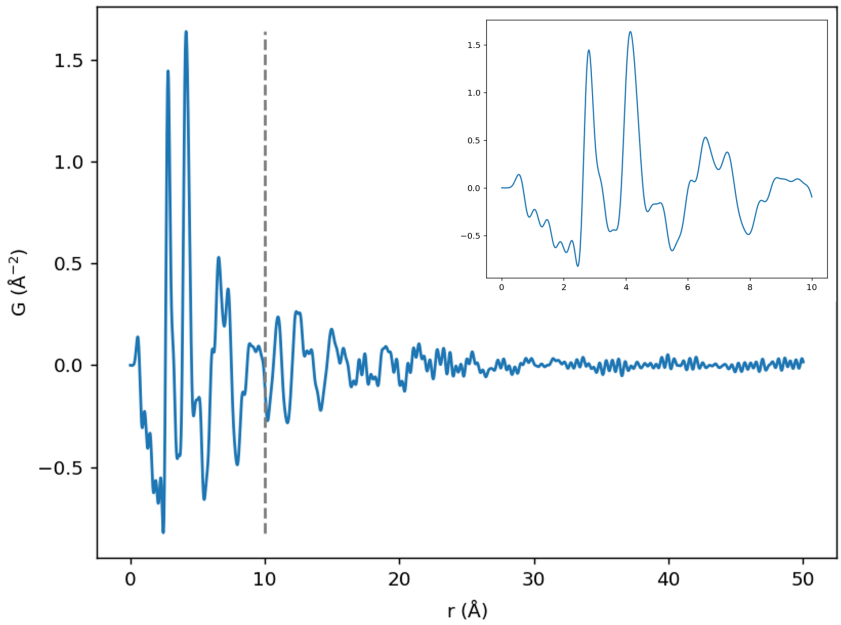

Figure 3.1 Experimental PDF data for amorphous Bi_2Se_3. The peaks below 30 Å correspond to well-defined short range order, while the relatively featureless behavior beyond 30 Å indicates random arrangement of atoms beyond that length scale.

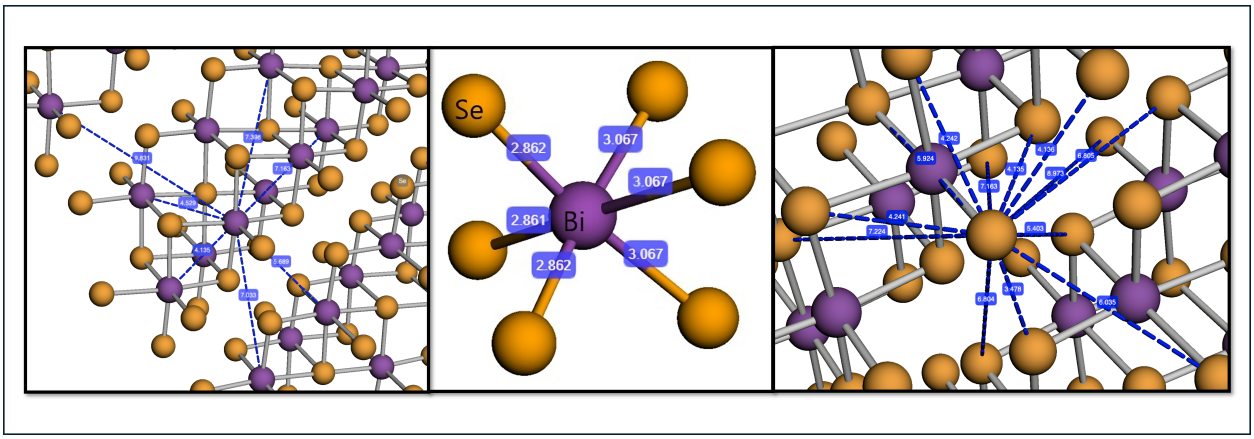

Figure 3.2 Distances between atoms for crystalline Bi_2Se_3. Bi-Bi (left), Bi-Se (middle), Se-Se (right).

dependent upon long range periodicity as previously assumed. Initial observation makes clear the fact that the topological state must stem more from local order than from long range periodictiy.

3.2 Small Box Modeling

The small box modeling described in Section 2.3 proved especially useful for evaluating the similarities and differences between crystalline and amorphous Bi_2Se_3. Correlations present between each variant's PDF point to the atomic configurations likely to be responsible for the preservation of spin-momentum locking, and thus the topological state, in amorphous Bi_2Se_3. Simulated crystalline Bi_2Se_3 was used to create PDFs that were fitted to PDFs garnered from experimentally gathered x-ray diffraction data that our amorphous Bi_2Se_3 sample produced. This method was the first step in uncovering the nature of amorphous Bi_2Se_3 structure.

Fig. 3.3 depicts a single unit cell of crystalline Bi_2Se_3. The positions of each atom in the unit cell are given by a CIF file, which can be expanded to arbitrary number of vertically and horizontally stacked unit cells. Recognizing that amorphous Bi_2Se_3 possesses local atomic order, we compared the fit between the PDF for experimentally acquired amorphous Bi_2Se_3 to a number of PDFs derived from varied simulated Bi_2Se_3 unit cell configurations to discover what local relationships are responsible for atomic order in amorphous Bi_2Se_3.

Fig. 3.4 presents a concise summary of these configurations. PDFs were generated for each of the unit cell configurations as outlined in the figure. Crystal Bi_2Se_3 PDFs are plotted in magenta, overlaid with experimental amorphous Bi_2Se_3 PDFs in blue. In all configurations, there is a close resemblance between the short-range features of the PDF for simulated crystal Bi_2Se_3 and that of amorphous Bi_2Se_3, making clear the similarities in local atomic order, but there are significant differences in many of them as well. To find the best fit, we varied the number of unit cells stacked in the in-plane and out-of-plane directions until we arrived at the minimal R_w value for fits between

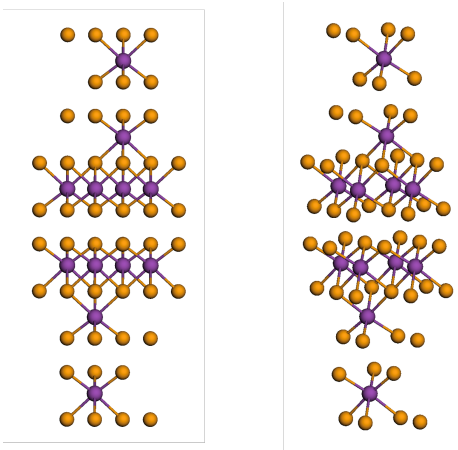

Figure 3.3 Single unit cell of crystalline Bi_2Se_3, depicted at two angles. Varying the number of simulated unit cells in both the horizontal and vertical directions, we produced a variety of PDFs to compare with experimentally gathered PDFs for amorphous Bi_2Se_3. Structural components that most contribute to the local order of amorphous were unearthed using this technique

the two PDFs. We found that three horizontal unit cells, just one half of a vertical unit cell deep, provided the PDF with the best fit to the experimental amorphous PDF. With this fit, the prominent peaks within ten angstroms of the amorphous Bi_2Se_3 PDF are captured generally by the simulated crystal PDF, signifying the necessity of short range order, which is likely responsible for preserving the topological state. The finer details of width, amplitude, and position, however, are slightly lost—increasingly with distance. Clearly some local order is requisite, but rigid crystal structure is not necessary, even on the short range, for the topological state to survive. Fits using linear combinations of various PDFs corroborate this result, as optimal weights were distributed between two and four unit cells wide and one deep, implying that three unit cells is the optimal configuration.

The results of small box modeling also clearly indicate that short range order is more dependent upon horizontal layers than it is vertical. Fig. 3.4 shows that vertical unit cells have more impact on long range order than on short range. Horizontal unit cells are responsible for the PDF correlations on the short range. Expansion beyond three horizontal unit cells is also not useful, as depicted by Fig. 3.5, which displays 10 vertical unit cells with one unit cell in the horizontal and one vertical

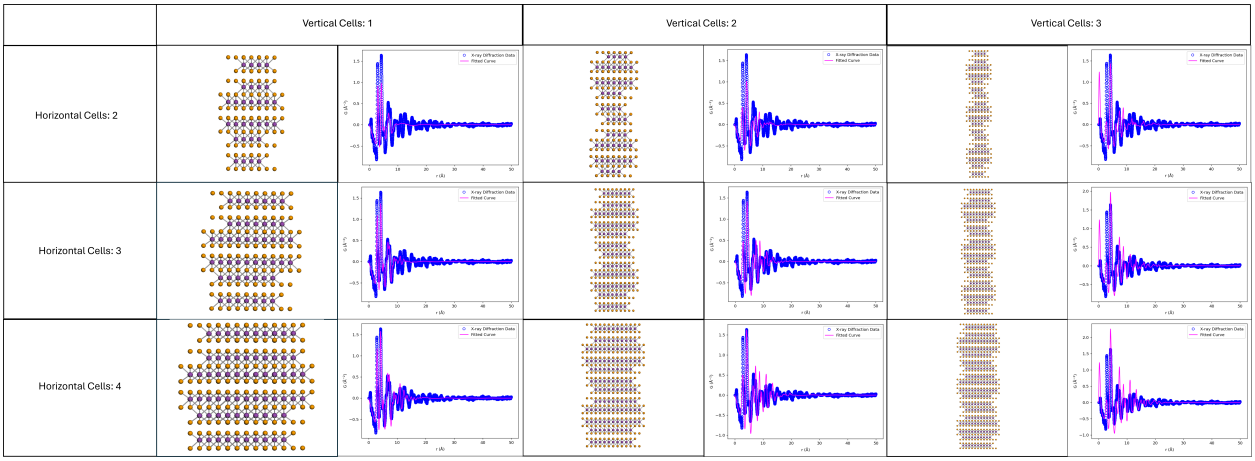

Figure 3.4 Variations of unit cell building blocks for crystalline Bi_2Se_3. Depicted is the effect on PDFs produced by combinations of 2, 3, or 4 horizontal unit cells, and 1, 2, or 3 vertical unit cells. Altering the width of the simulated material by adding unit cells horizontally produced a different effect than altering the depth of the simulated material by adding unit cells vertically.

unit cell with 10 unit cells in the horizontal. These configurations exaggerate the effect of both types of layering, revealing the effect that each has on the resulting PDF. The effects displayed by the magenta simulated crystal PDF overlaid with the experimental amorphous PDF make clear that local order is most dependent on in-plane correlations, and that those relationships are insignificant beyond about about 3 unit cells in amorphous Bi_2Se_3.

3.3 Large Box Modeling

To gain further insight into the structure of amorphous Bi_2Se_3, we employed RMC techniques as described in Section 2.3 to simulate large box models of amorphous Bi_2Se_3. Fig. 3.6 shows the configuration of a Bi_2Se_3 CIF file before and after applying the RMC method. Utilizing ORNL's rmcprofile software, we effectively generated CIF files detailing atomic positions that create quantitatively similar PDFs to those of experimentally obtained PDFs for Bi_2Se_3. The simulated amorphous Bi_2Se_3 slab depicted at right in Fig. 3.6 visualizes an atomic configuration that

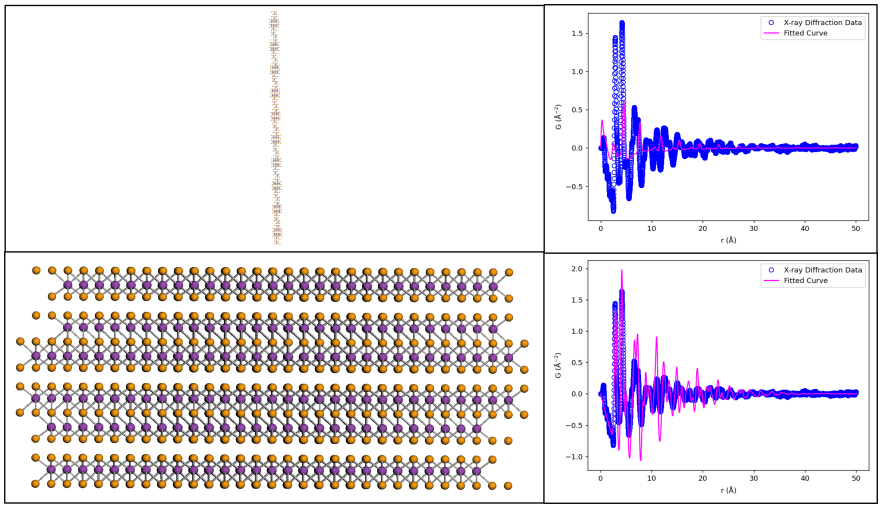

Figure 3.5 Ten vertical unit cells with one horizontal unit cell (top) and one vertical unit cell with ten horizontal unit cells (bottom). Vertical additions affect periodicity more on the long range, as the vertical distance in the unit cell is greater than the horizontal distance. Thus, horizontal additions have a greater impact on short range order than do vertical. However, amorphous Bi_2Se_3 only maintains this short range order out to approximately three horizontal unit cells as shown by Fig. 3.4. Using more than three, as shown by the figure above, does not represent the local order present in amorphous Bi_2Se_3

produced a PDF that matched the experimental amorphous Bi_2Se_3 PDF nearly perfectly. Since these atomic configurations generated PDFs of such strong fit to PDFs generated from amorphous Bi_2Se_3 x-ray diffraction data, we conclude that the simulated amorphous Bi_2Se_3 models are highly reliable, and accurately describe possible atomic positions that would host diffuse spin-momentum locking and the topologically insulating state. With these generated files, we averaged the coordination numbers and bond-angle distributions for 44 simulations of amorphous Bi_2Se_3, each providing information about how amorphization is realized within the material.

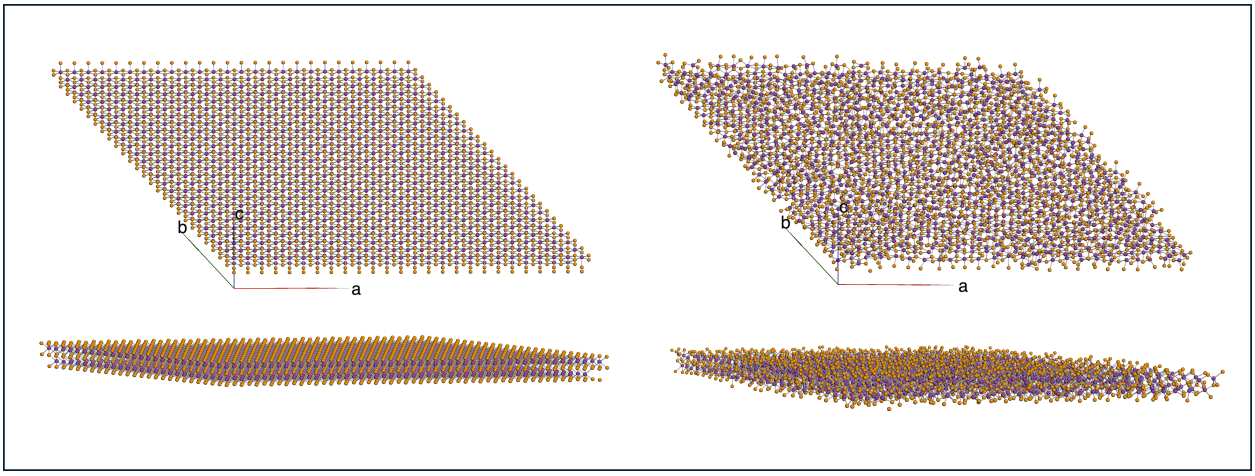

Figure 3.6 Simulated crystalline Bi_2Se_3 (left) and simulated amorphous Bi_2Se_3 created through rmcprofile (right).

The coordination number is the count of atoms a given distance away from a chosen atom within a unit cell. For a crystalline material, coordination numbers plot as increasing step functions, since a given radial distance from any chosen atom will contain a well-defined number of atoms. In amorphous Bi_2Se_3, plotting the coordination number yields less well-defined results, instead displaying a curve revealing the relative disruption in atomic configuration through the transition from crystalline to amorphous. Fig. 3.8 displays this curve for Bi_2Se_3. The preservation of bismuth-selenium interatomic distances is apparent as seen from the smooth bump appearing around the step function overlaid with this plot, which depicts the coordination number plot for crystalline

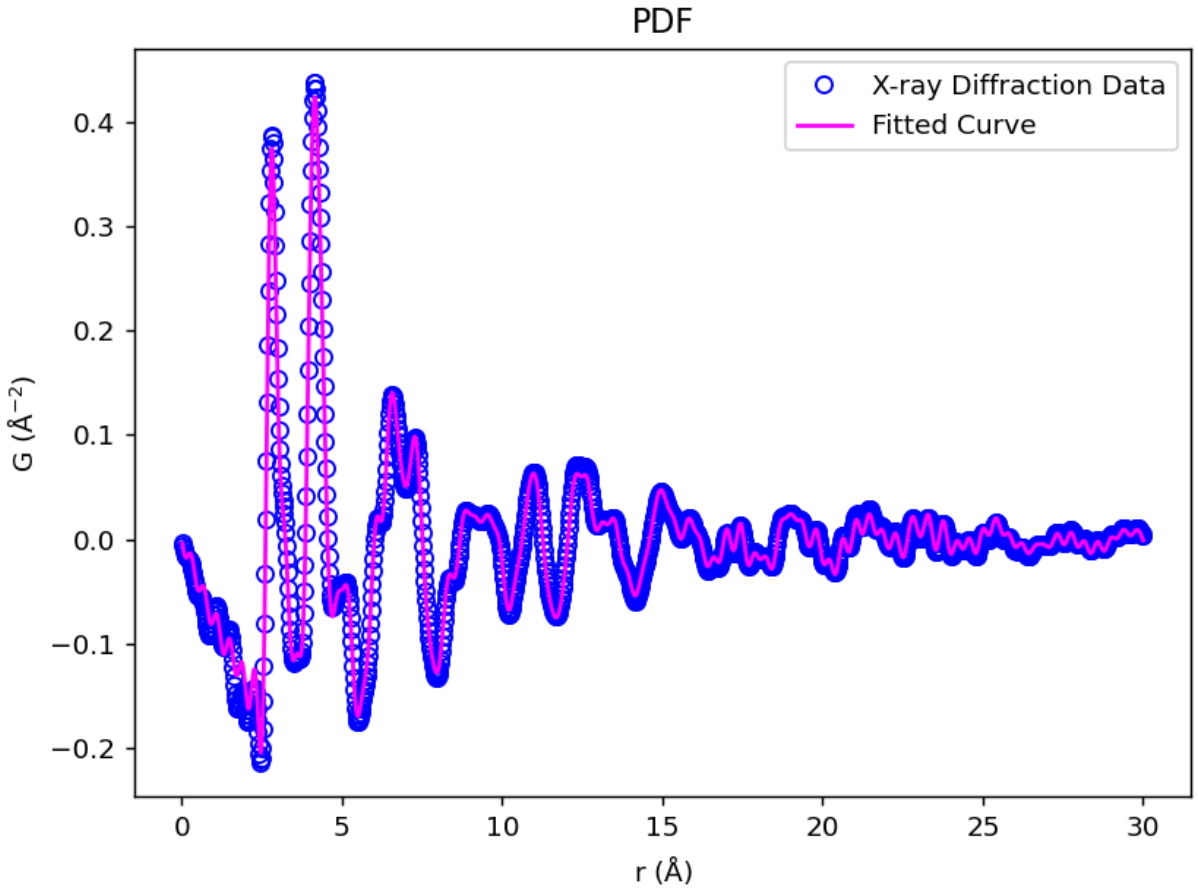

Figure 3.7 Fit between PDFs generated for experimental amorphous Bi_2Se_3 film (blue) and simulated amorphous Bi_2Se_3. The strong fit between the two implies a reliable simulation that can be utilized for further study.

Bi_2Se_3. The smooth curvature of the coordination number for RMC simulated crystal Bi_2Se_3 in blue is due to the random atomic shifts that occurred during mock-amorphization through rmcprofile. The shape of the curvature indicates that amorphization does not completely erase the unit cell construction of amorphous Bi_2Se_3, but certainly disrupts it. Interatomic distances become less defined, shifting away from their usually rigid distances, but maintaing a semblance of their former rigid crystalline structure, through the maintenance of near-neighbor distances.

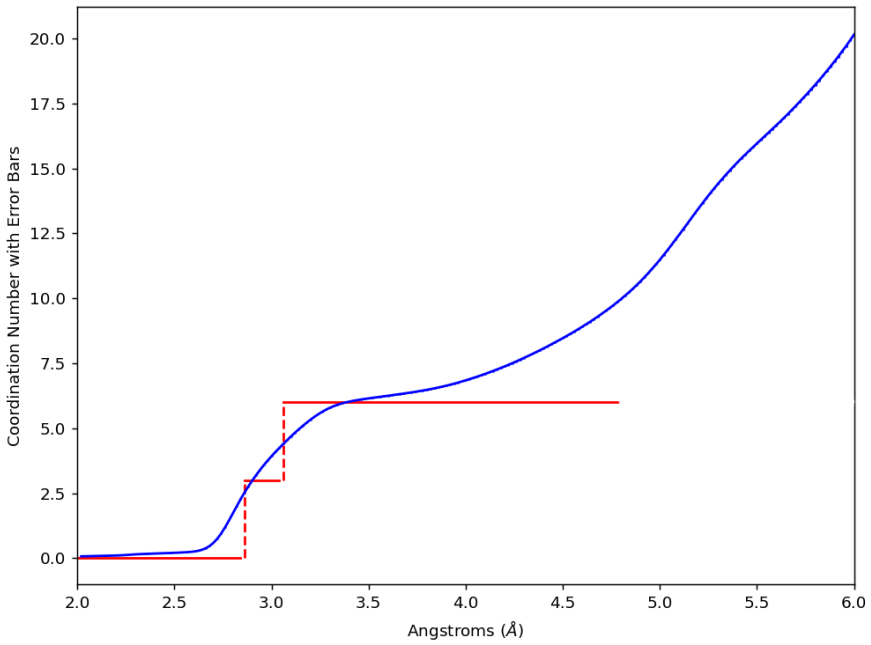

Figure 3.8 Coordination number for the distance from bismuth to selenium in an rmcprofile-generated amorphous Bi_2Se_3 simulation. The red step functions indicate the two nearest distances that selenium is expected to be found from bismuth in a unit cell of Bi_2Se_3. The curve does not display exponential growth, but rather a slowed growth surrounding these step functions, indicating the preservation of local order, especially within unit cells of Bi_2Se_3. Small error bars attest to the necessity of interatomic distances in amorphous Bi_2Se_3 only slightly less well-defined than what is expected for crystalline Bi_2Se_3.

Fig. 3.9 shows how angles between atomic triplets are altered by amorphization. Average bond counts for a given angle are displayed, with selenium-bismuth-selenium bonds depicted left (a) and

bismuth-selenium-bismuth depicted right (b). Dotted red lines mark the angles characteristic of rigid crystalline Bi_2Se_3. Amorphization widens these angles, resulting in one distribution of angles around 90 degrees, and a smaller distribution near 180 degrees. The majority of bonds occur at nearly right angles in crystal Bi_2Se_3, so this result is expected.

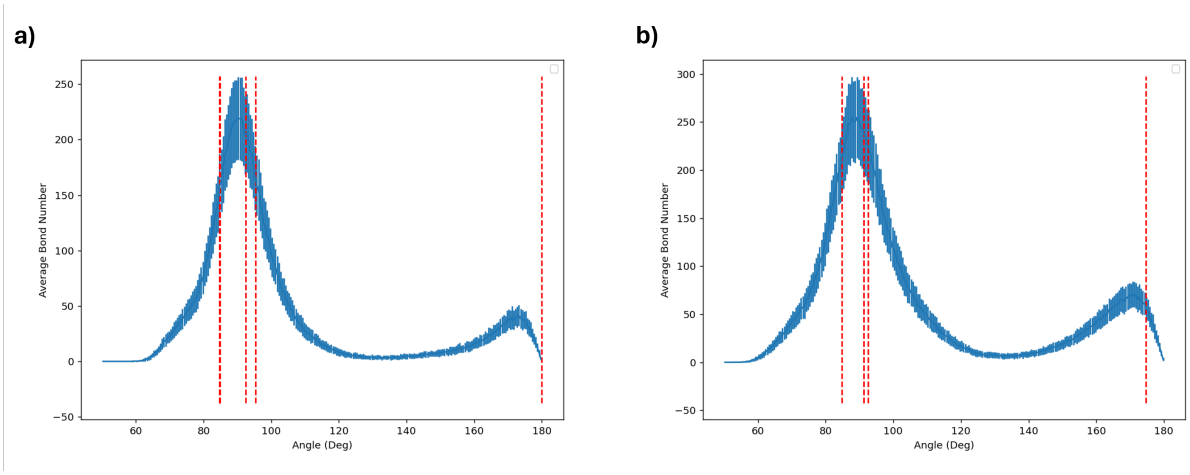

Figure 3.9 Distribution of bond angles for Bi-Se-Bi (a) and Se-Bi-Se (b). Red lines indicate bond angles expected for each triplet in crystalline Bi_2Se_3. Amorphization tends to spread these expected angles into roughly average distributions around expected angles. Large error bars suggest that bond angle distribution is less significant than interatomic distance.

These two data sets unveil more atom-specific detail regarding the configuration of amorphous Bi_2Se_3. Coordination numbers reveal that the interatomic distance between atom-pairs remains quite similar to what is expected from crystalline Bi_2Se_3, with minor contraction and expansion of the material visible due to amorphization. The distance between bismuth and selenium remains virtually the same for any RMC simulation of amorphous Bi_2Se_3, as shown by the almost negligible error plotted with the coordination number averages. Fig. 3.8 clearly expresses the preservation of interatomic distances despite deformation.

Bond angle distributions are subject to more unpredictable deformation. While the peaks of these distributions demonstrates that bond angles remain generally the same between amorphous and crystalline Bi_2Se_3, the large error bars suggest that a massive number of possible distributions

result in a PDF that is similar to the experimentally gathered PDF for amorphous Bi_2Se_3. So long as the short range atomic distances, given by the coordination number plot, remain within an acceptable range, the bond angles at which this is accomplished has little significance.

Chapter 4

Discussion

4.1 Extant Topological Insulation in Amorphous Material

While traditionally topological insulators have been predominantly associated with crystalline structures, the emergence of spin-momentum locked surface states in amorphous materials defies conventional expectations. Our research begins to bridge this gap by scrutinizing the behavior of topologically insulating states in amorphous Bi_2Se_3. Meticulous characterization of the structure of amorphous Bi_2Se_3 thin films elucidates the distinctive features governing the stability of topological states in disordered topological insulators. This investigation paves the way for the development of comprehensive theoretical frameworks that expand current descriptions to encompass amorphous topological insulators.

The intriguing preservation of topological insulation despite the transition from crystalline to amorphous structure led naturally to the exploration of short-range inter-atomic distances and bond angles distributions that uniquely characterize amorphous Bi_2Se_3. Creating small and large box models matching results to fine-grain x-ray diffraction data proved an excellent tool for discovering exactly what those distances and distributions were, and reliably produced the error within which

plausible atomic configurations would still result in the preservation of the topologically insulating state. The data paints a picture of starkly amorphous Bi_2Se_3 with intra-layer correlations reminiscent of crystalline Bi_2Se_3. This reminiscence stamps itself on the data gathered from small box models which demonstrated the reliance on unit cell configurations across horizontal expansions of the material, as opposed to vertical layer depths. Further, large box models produced by the RMC method resulted in an understanding of the sturdy yet flexible nature of Bi_2Se_3 unit cells, which tend to preserve their local relationships through amorphization.

4.2 Simulations Interpreted

Analysis of the coordination number distributions obtained from our experiments reveals that even through amorphization, the local environment surrounding each atom maintains a consistent number of nearest neighbors. This observation underscores the robustness of short-range order in amorphous Bi_2Se_3, suggesting that annealing does not significantly disrupt the coordination of atoms. Moreover, our examination of the bond angle distribution unveils a distinct trend: under annealing conditions, bonds within the material tend to buckle, resulting in a decrease in interatomic distances. This phenomenon is accompanied by a deviation of bond angles from the ideal 180 degrees, indicative of structural rearrangements that accompany changes in local order. The changes in bond geometry and interatomic distance induced by annealing yield a deeper understanding of the structural dynamics of amorphous Bi_2Se_3, with implications for the design and optimization of materials for various applications in electronics, spintronics, lossless transisting for quantum computing, and beyond.

4.3 Further Study

Our research outcomes offer essential and intricate insights into the fundamental physical properties of Bi_2Se_3. Through careful analysis, we have observed the material's remarkable tendency to uphold short-range order even through amorphization, and even presumably through synthesis that produces irregular or imperfect samples—a finding of paramount importance in material science, specifically for the implication that flawless synthesis is not required to obtain the desired function of these materials.

While potential applications are exciting, refined theoretical understanding will be equally beneficial to the community. A stronger understanding of these unique topological states will prove useful for predicting and identifying future topological insulators. The ability to better characterize these materials once discovered will permit their use in broader applications and perhaps even in cheaper and easier production.

List of Figures

Bibliography

[1] "Topological insulator," https://en.wikipedia.org/wiki/Topological_insulator#cite_note-Volkov85-12 (Accessed Feb 16, 2024).

[2] O. Knill, "Lecture 9: Topology," https://people.math.harvard.edu/~knill/teaching/mathe320_2022/handouts/08 topology.pdf (2010).

[3] J. E. Moore, "The birth of topological insulators," Nature **464,** 194–198 (2010).

[4] P. Corbae *et al.*, "Observation of spin-momentum locked surface states in amorphous Bi2Se3," Nature Materials **22,** 200–206 (2023).

[5] B. A. Volkov and O. A. Pankratov, "Two-dimensional massless electrons in an inverted contact," JETPL **42,** 145 (1985).

[6] B. A. Bernevig, T. L. Hughes, and S.-C. Zhang, "Quantum Spin Hall Effect and Topological Phase Transition in HgTe Quantum Wells," Science **314,** 1757–1761 (2006).

[7] M. Konig, S. Wiedmann, C. Brune, A. Roth, H. Buhmann, L. W. Molenkamp, X.-L. Qi, and S.-C. Zhang, "Quantum Spin Hall Insulator State in HgTe Quantum Wells," Science **318,** 766–770 (2007).

[8] D. Hsieh, D. Qian, L. Wray, Y. Xia, Y. S. Hor, R. J. Cava, and M. Z. Hasan, "A topological Dirac insulator in a quantum spin Hall phase," Nature **452,** 970–974 (2008).

[9] Y. X. Xia *et al.*, "Observation of a large-gap topological-insulator class with a single Dirac cone on the surface," Nature Physics **5,** 398–402 (2009).

[10] M. Z. Hasan and J. E. Moore, "Three-Dimensional Topological Insulators," Annual Review of Condensed Matter Physics **2,** 55–78 (2011).

[11] B. Wu, J. Song, J. Zhou, and H. Jiang, "Disorder effects in topological states: Brief review of the recent developments," Chinese Physics B 25 (2016), cited by: 29; All Open Access, Green Open Access.

[12] K. Sumida, Y. Ishida, J. Güdde, U. Höfer, S. Shin, and A. Kimura, "Ultrafast surface Dirac fermion dynamics of Sb2Te3-based topological insulators," Progress in Surface Science **96,** 100628–100628 (2021).